Article:
Lesnic, D and Alosaimi, M (2023) Determination of the space-dependent blood perfusion coefficient in the thermal-wave model of bio-heat transfer. Engineering Computations, 40 (2). pp. 411-433. ISSN: 0264-4401

https://doi.org/10.1108/EC-07-2022-0467

Determination of the space-dependent blood perfusion coefficient in the thermal-wave model of bio-heat transfer

Abstract. This paper aims to retrieve the space-dependent blood perfusion coefficient in the thermal-wave model of bio-heat transfer from final time temperature measurement. This non-linear and ill-posed problem is reformulated as a non-linear minimization problem of a Tikhonov regularization functional subject to lower and upper simple bounds on the unknown coefficient. For the numerical discretization, an unconditionally stable direct solver based on the Crank-Nicolson finite-difference scheme is developed. The Tikhonov regularization functional is minimized iteratively by the built-in routine *lsqnonlin* from the MATLAB optimization toolbox. The reconstruction of the unknown blood perfusion coefficient for three benchmark numerical examples is illustrated and discussed to verify the proposed numerical procedure. Moreover, the proposed algorithm is tested on a physical example which consists of identifying the blood perfusion rate of a biological tissue subjected to an external source of laser irradiation.

Keywords: Inverse problem; bio-heat transfer; blood perfusion coefficient; Tikhonov regularization; thermal-wave model

1. Introduction

Heat transfer in biological bodies is driven by processes such as conduction, blood perfusion and heat generation due to metabolism [18]. The widely used Pennes' bio-heat model [28] implies that (as it is based on the classical Fourier's law) any thermal change in the medium is felt instantaneously at all locations, i.e. an infinite speed of thermal propagation occurs. The Pennes' bio-heat parabolic PDE model [28] has proved sufficiently accurate to approximate a wide range of physical applications such as the prediction of temperature evolution during cancer's hyperthermia [32], estimation of thermal effects of radiation from cellular phones [41], the use of thermal therapies for the ablation of diseased tissues [17], etc. However, when modelling heat propagation in biological bodies, a non-negligible relaxation time (typically between 15-30 seconds) is required for the thermal waves to accumulate and transfer, i.e. thermal waves propagate at a finite velocity, [7, 24, 29]. Cattaneo [9] and Vernotte [40] independently modified Fourier's law to account for such a realistic and physical feature. Such extension has been the basis of the thermal-wave model of bio-heat transfer given by, [20],

$$\rho_{\mathrm{t}} c_{\mathrm{t}} \tau \frac{\partial^2 T}{\partial t^2} + (\rho_{\mathrm{t}} c_{\mathrm{t}} + \tau \rho_b c_b w_b) \frac{\partial T}{\partial t} = k \nabla^2 T + \rho_b c_b w_b (T_a - T) + Q_m + Q_e + \tau \frac{\partial}{\partial t}(Q_m + Q_e), \quad (1)$$

where T, ρ_{t}, c_{t} and k are the temperature [K or °C], density [kg/m^3], specific heat [J/(kg K) or J/(kg °C)] and thermal conductivity [W/(m K) or W/(m °C)] of the tissue, respectively, ρ_b, c_b and w_b stand for the density [kg/m^3], specific heat [J/(kg K) or J/(kg °C)] and perfusion rate [s^{-1}] of the blood, respectively, τ is the relaxation time [s], ∇^2 is the Laplace operator, t is the time [s] and T_a is the (arterial) blood temperature [K or °C]. The sources Q_m and Q_e are heat generations due to metabolism and external heating [W/m^3],

respectively. In the model (1), $\tau = \alpha/\mathrm{c}^2$, where $\alpha = k/(\rho_\mathrm{t} c_\mathrm{t})$ is the thermal diffusivity of the tissue [m^2/s] and c is the velocity of thermal waves [m/s], [24].

Research in coefficient identification has been concerned with reconstructing the blood perfusion with various dependencies, e.g. constant, time-wise, space-wise, space- and time-wise or temperature-dependent [6, 8, 13, 35, 36, 37, 38, 39]. These studies have been possible only through the use of numerical optimization methods and were based on the Pennes' bio-heat parabolic model. Although these studies estimated an important thermo-physical parameter, they neglected the wave-like nature of heat conduction present in biological tissues and captured by the thermal-wave model of bio-heat transfer [1]. The novelty and objective of this paper are to account for such a more accurate thermal-wave bio-heat model and investigate the possibility of determining its space-dependent blood perfusion coefficient from temperature measurements at the final time.

This paper is organized as follows. The mathematical formulation of the inverse problem of identifying the space-dependent perfusion coefficient along with the temperature is undertaken in Section 2. In Section 3, the finite-difference method (FDM) used as a direct solver, is discussed, while the numerical optimization approach for inversion is presented in Section 4. Numerical benchmark examples for identifying blood perfusion coefficients of different nature are illustrated and discussed in Section 5, along with a physical example concerning the estimation of the blood perfusion rate of a biological tissue subjected to an external source of laser irradiation. Section 6 highlights the conclusions of this work.

2. Mathematical formulation

We investigate the governing hyperbolic partial differential equation (1) subject to appropriate initial and boundary conditions when the unknown perfusion coefficient $w_b(x)$ is not constant, but it depends on the space variable. Therefore, this generality allows extending previous analyses [3, 4, 5] by the authors to investigate heterogeneous tissues which are more general/realistic than the homogeneous ones. For simplicity, all the other thermal parameters are assumed to be known and constant, and we shall consider the one-dimensional time-dependent case only although a similar analysis holds also in higher dimensions.

Letting L [m] denote the length of the finite tissue slab and t_f [s] a time duration of interest, then equation (1) simplifies to, [21],

$$C_\mathrm{t}\tau\frac{\partial^2 T}{\partial t^2}(x,t) + \big(C_\mathrm{t} + \tau C_b w_b(x)\big)\frac{\partial T}{\partial t}(x,t) = k\frac{\partial^2 T}{\partial x^2}(x,t) - C_b w_b(x)(T - T_a) + Q_m + Q_e + \tau\frac{\partial}{\partial t}(Q_m + Q_e), \quad (x,t) \in (0,L)\times[0,t_\mathrm{f}], \quad (2)$$

where $C_\mathrm{t} \coloneqq \rho_\mathrm{t} c_\mathrm{t}$ [$\mathrm{J}/(\mathrm{m}^3\ \mathrm{K})$ or $\mathrm{J}/(\mathrm{m}^3\ ^\circ\mathrm{C})$] and $C_b \coloneqq \rho_b c_b$ [$\mathrm{J}/(\mathrm{m}^3\ \mathrm{K})$ or $\mathrm{J}/(\mathrm{m}^3\ ^\circ\mathrm{C})$] are the heat capacities of tissue and blood, respectively.

We consider the hyperbolic partial differential equation (2) subject to the initial conditions

$$T(x,0) = \phi(x), \quad \frac{\partial T}{\partial t}(x,0) = \psi(x), \quad x \in [0,L], \quad (3)$$

where ϕ and ψ are prescribed functions, and the convective Robin boundary conditions

$$\begin{aligned} -k\frac{\partial T}{\partial x}(0,t) &= h_0(t)(T_{\infty,0}(t) - T(0,t)), \quad t \in [0,t_{\rm f}], \\ k\frac{\partial T}{\partial x}(L,t) &= h_L(t)(T_{\infty,L}(t) - T(L,t)), \quad t \in [0,t_{\rm f}], \end{aligned} \tag{4}$$

where h_0 and h_L are heat transfer (exchange) coefficients [W/(m^2 K) or W/(m^2 °C)] at the boundaries $x = 0$ and $x = L$, respectively, and $T_{\infty,0}$ and $T_{\infty,L}$ are the ambient temperatures [K or °C] outside the boundaries $x = 0$ and $x = L$, respectively.

As an additional measurement to compensate for the missing knowledge of $w_b(x)$, we consider specifying the final time temperature

$$T(x,t_{\rm f}) = T_{t_{\rm f}}(x), \quad x \in [0,L], \tag{5}$$

where $T_{t_{\rm f}}$ is a prescribed function. Alternatively, one could measure the boundary temperature

$$T(0,t) = \mu_1(t), \quad t \in [0,t_{\rm f}], \tag{6}$$

or

$$T(L,t) = \mu_2(t), \quad t \in [0,t_{\rm f}], \tag{7}$$

such that from (4), partial Cauchy boundary data would be prescribed, [14, 22, 33, 42], the partial interior observation

$$T(x,t) =: \mathcal{T}(x,t), \quad (x,t) \in \omega \times (0,t_{\rm f}], \tag{8}$$

where ω is a subdomain of $(0,L)$, [15], or the time-average temperature specification

$$\int_0^{t_f} \chi(t)T(x,t)dt = E(x), \quad x \in [0,L], \tag{9}$$

where χ is a given function, [19].

Uniqueness results for the pair of functions $\big(w_b(x), T(x,t)\big)$ satisfying the inverse problem given by equation (2) with $\tau = 0$, i.e. the Pennes' bio-heat parabolic equation

$$C_{\rm t}\frac{\partial T}{\partial t}(x,t) = k\frac{\partial^2 T}{\partial x^2}(x,t) - C_b w_b(x)(T - T_a) + Q_m + Q_e, \quad (x,t) \in (0,L) \times [0,t_{\rm f}], \tag{10}$$

initial condition

$$T(x,0) = \phi(x), \quad x \in [0,L], \tag{11}$$

Dirichlet boundary conditions (6), (7) and the extra measurement (5) of the temperature or the heat flux

$$-k\frac{\partial T}{\partial x}(0,t) = q_0(t) \quad \text{or} \quad k\frac{\partial T}{\partial x}(L,t) = q_L(t), \quad t \in [0,t_{\rm f}] \tag{12}$$

are provided in [16] and [31], respectively. On the other hand, for the hyperbolic inverse problem (2)–(5), or (2), (3), (5)–(7), or (2)–(4), (6), or (2)–(4), (7), uniqueness results are

not known yet, but they could be investigated in the future using, e.g. the techniques from [19] (Carleman estimates) and Chapter 8 of [30] (semi-group theory).

The thermal-wave model of bio-heat transfer (2)–(5) can be non-dimensionalized, as follows. Assuming that T_a is a non-zero constant, we introduce the following dimensionless variables:

$$\begin{aligned}
&(\bar{x}, \mathrm{L}) = \sqrt{\frac{C_\mathrm{t}}{k\tau}}(x, L), \quad (\bar{t}, \mathrm{t_f}) = \frac{1}{\tau}(t, t_\mathrm{f}), \quad u = \frac{T - T_a}{T_a}, \quad \bar{\phi} = \frac{\phi - T_a}{T_a}, \\
&\bar{\psi} = \frac{\tau\psi}{T_a}, \quad u_{\infty,0} = \frac{T_{\infty,0} - T_a}{T_a}, \quad u_{\infty,\mathrm{L}} = \frac{T_{\infty,L} - T_a}{T_a}, \quad u_{\mathrm{t_f}} = \frac{T_{t_\mathrm{f}} - T_a}{T_a}, \\
&\big(\bar{h}_0, \bar{h}_\mathrm{L}\big) = \sqrt{\frac{\tau}{kC_\mathrm{t}}}(h_0, h_L), \quad F = \frac{\tau(Q_e + Q_m)}{T_a C_\mathrm{t}}, \quad w = \frac{\tau C_b w_b}{C_\mathrm{t}}.
\end{aligned} \tag{13}$$

Then, the dimensionless form of the thermal-wave model (2)–(5) (omitting the bars for clarity and denoting $f = F + F_t$) can be written as

$$\begin{aligned}
\frac{\partial^2 u}{\partial t^2}(x,t) + \big(1 + w(x)\big)\frac{\partial u}{\partial t}(x,t) = \frac{\partial^2 u}{\partial x^2}(x,t) - w(x)u(x,t) + f(x,t), \\
(x,t) \in \Omega_{\mathrm{t_f}} \coloneqq (0, \mathrm{L}) \times [0, \mathrm{t_f}],
\end{aligned} \tag{14}$$

subject to the initial conditions

$$u(x,0) = \phi(x), \quad \frac{\partial u}{\partial t}(x,0) = \psi(x), \quad x \in [0, \mathrm{L}], \tag{15}$$

the convective Robin boundary conditions

$$\begin{aligned}
-\frac{\partial u}{\partial x}(0,t) = h_0(t)\big(u_{\infty,0}(t) - u(0,t)\big), \quad \frac{\partial u}{\partial x}(\mathrm{L},t) = h_\mathrm{L}(t)\big(u_{\infty,\mathrm{L}}(t) - u(\mathrm{L},t)\big), \\
t \in [0, \mathrm{t_f}],
\end{aligned} \tag{16}$$

and the final time temperature

$$u(x, \mathrm{t_f}) = u_{\mathrm{t_f}}(x), \quad x \in [0, \mathrm{L}]. \tag{17}$$

In the particular case that the ambient temperatures $T_{\infty,0}$ and $T_{\infty,L}$ are constant and equal to the arterial temperature T_a, and that the heat transfer coefficients h_0 and h_L are also constant, the boundary conditions (16) simplify as

$$-\frac{\partial u}{\partial x}(0,t) + h_0 u(0,t) = 0, \quad \frac{\partial u}{\partial x}(\mathrm{L},t) + h_\mathrm{L} u(\mathrm{L},t) = 0, \quad t \in [0, \mathrm{t_f}], \tag{18}$$

and the problem (14), (15), (17) and (18) can be seen as a one-dimensional model of the more general higher-dimensional setting of the inverse problem given by

$$\frac{\partial^2 u}{\partial t^2}(x,t) + \big(1 + w(x)\big)\frac{\partial u}{\partial t}(x,t) = \nabla^2 u(x,t) - w(x)u(x,t) + f(x,t),$$

$$(x,t) \in D \times [0, \mathrm{t_f}], \tag{19}$$

$$u(x,0) = \phi(x), \quad \frac{\partial u}{\partial t}(x,0) = \psi(x), \quad x \in D, \tag{20}$$

$$\frac{\partial u}{\partial n}(x,t) + h(x)u(x,t) = 0, \quad (x,t) \in \partial D \times [0, \mathrm{t_f}], \tag{21}$$

$$u(x, \mathrm{t_f}) = u_{\mathrm{t_f}}(x), \quad x \in D, \tag{22}$$

where D is a bounded domain in $\mathbb{R}^d$, $(d = 1, 2, 3)$, with sufficiently smooth boundary ∂D of outward unit normal $\mathbf{n}$, $h = h(x)$ is a given, sufficiently smooth, time-independent boundary heat transfer coefficient, $f \in C([0, \mathrm{t_f}]; L^2(D))$, $\phi \in H^1(D)$ and $\psi \in L^2(D)$ are given data, $w \in C^2(\overline{D})$ and $u_{\mathrm{t_f}} \in \mathcal{D}(\mathcal{A})$, where

$$\mathcal{D}(\mathcal{A}) = \left\{ \boldsymbol{U} = \begin{pmatrix} u \\ \mathrm{v} \end{pmatrix} \in H^2(D) \times H^1(D); \left(\frac{\partial u}{\partial n} + hu \right) \Big|_{\partial D} = 0 \right\}, \tag{23}$$

is the domain of the operator

$$\mathcal{A} = \begin{pmatrix} -I & I \\ \nabla^2 & -wI \end{pmatrix} \tag{24}$$

acting on the space $X = H^1(D) \times L^2(D)$ equipped with the family of equivalent norms, see p.590 of [30],

$$|||\boldsymbol{U}|||^2 = \|\nabla u\|^2_{L^2(D)} + \beta \|u\|^2_{L^2(D)} + \|\mathrm{v}\|^2_{L^2(D)} + \int_{\partial D} h(x) u^2(x) ds, \tag{25}$$

for $\beta > 0$ sufficiently large. The operator $\mathcal{A}$ is closed and its domain of definition (23) is dense in the space X. On rewriting (19) as the system

$$\begin{cases} u_t = \mathrm{v} - u, \\ \mathrm{v}_t = \nabla^2 u - w(x)\mathrm{v} + f(x,t), \end{cases} \tag{26}$$

we can view the direct problem (19)–(21) as the abstract Cauchy problem

$$\begin{cases} \boldsymbol{U}'(t) = \mathcal{A}\boldsymbol{U}(t) + \mathbf{F}(t), \quad t \in [0, \mathrm{t_f}], \\ \boldsymbol{U}(0) = \boldsymbol{U}_0, \end{cases} \tag{27}$$

where $\mathcal{A}$ is given by (24), $\boldsymbol{U}(t) = (u, \mathrm{v})^{\mathrm{T}}$, $\mathbf{F} = (0, f)^{\mathrm{T}}$ and $\boldsymbol{U}_0 = (\phi, \phi + \psi)^{\mathrm{T}}$.

Remark 1. (Case of Dirichlet boundary conditions)
In case of homogeneous Dirichlet boundary conditions

$$u(0,t) = u(\mathrm{L},t) = 0, \quad t \in [0,\mathrm{t_f}], \tag{28}$$

obtained when μ_1 *and* μ_2 *in* (6) *and* (7) *are constant and equal to* T_a*, or its higher-dimensional form*

$$u(x,t) = 0, \quad (x,t) \in \partial D \times [0,\mathrm{t_f}], \tag{29}$$

in place of the homogeneous Robin boundary conditions (21)*, the domain of the operator* $\mathcal{A}$ *and the space* X *simplify as* $\mathcal{D}(\mathcal{A}) = (H^2(D) \cap H_0^1(D)) \times H_0^1(D)$ *and* $X = H_0^1(D) \times L^2(D)$ *equipped with the usual family of norms*

$$|||\boldsymbol{U}|||^2 = \|u\|^2_{H^1(D)} + \|\mathrm{v}\|^2_{L^2(D)}. \tag{30}$$

To advance the theoretical analysis one could possibly make use of the theory of semi-groups to show that, under certain conditions, the operator $\mathcal{A}$ defined by (24) is the infinitesimal generator of a C_0-group of bounded linear operators in the space X, see [27, pp.220-222], but this is not yet available. Instead we solve numerically the inverse coefficient problem in the non-dimensional thermal-wave model of bio-heat transfer (14)–(17) for reconstructing the temperature $u(x,t)$ and the space-dependent blood perfusion coefficient $w(x) = \tau w_b(x) C_b / C_{\mathrm{t}}$.

Before we proceed with the inversion in Section 4, in the next Section 3, we solve the linear and well-posed direct problem (14)–(16) when the blood perfusion coefficient $w(x)$ is assumed to be known using an unconditionally stable FDM based on the Crank-Nicolson scheme. Furthermore, the convergence of the FDM direct solver is verified on a benchmark example.

3. Numerical solution of direct problem

Before attempting to solve the non-linear and ill-posed inverse problem (14)–(17), we describe the numerical solution of the linear and well-posed direcy problem given by equations (14)–(16) when the blood perfusion coefficient $w(x)$ is assumed to be known.

We introduce the intermediate variable v, [11], as

$$v(x,t) \coloneqq \frac{\partial u}{\partial t}(x,t) + \big(1 + w(x)\big)u(x,t), \quad (x,t) \in \Omega_{\mathrm{t_f}}. \tag{31}$$

Then, equation (14) rewrites as

$$\frac{\partial v}{\partial t}(x,t) = \frac{\partial^2 u}{\partial x^2}(x,t) - w(x)u(x,t) + f(x,t), \quad (x,t) \in \Omega_{\mathrm{t_f}}. \tag{32}$$

From (15) and (31) we obtain the initial condition

$$v(x,0) = \psi(x) + \big(1 + w(x)\big)\phi(x), \quad x \in [0,\mathrm{L}]. \tag{33}$$

An alternative to the above split (31) and (32) could be given by $\tilde{v} \coloneqq u_t + w(x)u$ and $\tilde{v}_t + \tilde{v} = u_{xx} + f(x,t)$.

We subdivide the computational domain $\Omega_{\mathrm{t_f}}$ into M and N subintervals of equal mesh sizes $\Delta x = \mathrm{L}/M$ and uniform time step $\Delta t = \mathrm{t_f}/N$, respectively. At the node (x_i, t_j), we denote $u_{i,j} \coloneqq u(x_i,t_j)$, $v_{i,j} \coloneqq v(x_i,t_j)$, $w_i \coloneqq w(x_i)$, $h_0^j \coloneqq h_0(t_j)$, $h_{\mathrm{L}}^j \coloneqq h_{\mathrm{L}}(t_j)$, $u_{\infty,0}^j \coloneqq u_{\infty,0}(t_j)$, $u_{\infty,\mathrm{L}}^j \coloneqq u_{\infty,\mathrm{L}}(t_j)$ and $f_{i,j} \coloneqq f(x_i,t_j)$, where $x_i = i\Delta x$ and $t_j = j\Delta t$ for $i = \overline{0,M}$ and $j = \overline{0,N}$.

The Crank-Nicolson method, which is unconditionally stable and second-order accurate, discretizes (31) and (32) as

$$\begin{aligned}\frac{u_{i,j+1}-u_{i,j}}{\Delta t} &= \frac{1}{2}\big(v_{i,j} - (1+w_i)u_{i,j} + v_{i,j+1} - (1+w_i)u_{i,j+1}\big),\\ &\qquad i = \overline{0,M}, \quad j = \overline{0,(N-1)}, \qquad (34)\\ \frac{v_{i,j+1}-v_{i,j}}{\Delta t} &= \frac{1}{2}\left(\frac{1}{(\Delta x)^2}\delta_x^2 u_{i,j} - w_i u_{i,j} + f_{i,j} + \frac{1}{(\Delta x)^2}\delta_x^2 u_{i,j+1} - w_i u_{i,j+1} + f_{i,j+1}\right),\\ &\qquad i = \overline{0,M}, \quad j = \overline{0,(N-1)}, \qquad (35)\end{aligned}$$

where $u_{-1,j} = u(-\Delta x, t_j)$ and $u_{M+1,j} = u(\mathrm{L}+\Delta x, t_j)$ for $j = \overline{0,N}$, and $\delta_x^2 u_{i,j} \coloneqq u_{i-1,j} - 2u_{i,j} + u_{i+1,j}$.

Equations (15) and (33) are discretized as

$$u_{i,0} = \phi(x_i), \quad v_{i,0} = \psi(x_i) + (1+w_i)\phi(x_i), \quad i = \overline{0,M}, \qquad (36)$$

and equation (16) is discretized as

$$-\frac{u_{1,j}-u_{-1,j}}{2(\Delta x)} = h_0^j\Big(u_{\infty,0}^j - u_{0,j}\Big), \quad \frac{u_{M+1,j}-u_{M-1,j}}{2(\Delta x)} = h_{\mathrm{L}}^j\Big(u_{\infty,\mathrm{L}}^j - u_{M,j}\Big), \quad j = \overline{0,N}. \qquad (37)$$

Solving (34) for $v_{i,j+1}$, we obtain

$$v_{i,j+1} = \left(1 + w_i + \frac{2}{\Delta t}\right)u_{i,j+1} + \left(1 + w_i - \frac{2}{\Delta t}\right)u_{i,j} - v_{i,j}, \qquad (38)$$

for $i = \overline{0,M}$, $j = \overline{0,(N-1)}$. Introducing (38) in (35), we obtain

$$\begin{aligned}-Au_{i-1,j+1} + B_i u_{i,j+1} - Au_{i+1,j+1} =& Au_{i-1,j} + C_i u_{i,j} + Au_{i+1,j} + 2v_{i,j}\\ &+ \frac{\Delta t}{2}\big(f_{i,j} + f_{i,j+1}\big), \qquad (39)\end{aligned}$$

for $i = \overline{0,M}$, $j = \overline{0,(N-1)}$, where $A \coloneqq \dfrac{\Delta t}{2(\Delta x)^2}$, $B_i \coloneqq \left(\dfrac{2}{\Delta t} + \dfrac{\Delta t}{(\Delta x)^2} + 1\right) + \left(1 + \dfrac{\Delta t}{2}\right)w_i$ and $C_i \coloneqq \left(\dfrac{2}{\Delta t} - \dfrac{\Delta t}{(\Delta x)^2} - 1\right) - \left(1 + \dfrac{\Delta t}{2}\right)w_i$ for $i = \overline{0,M}$.

At each time step $t_{j+1} = (j+1)\Delta t$ for $j = \overline{0,(N-1)}$, incorporating the discretized

boundary conditions given by (37), the difference equations given by (38) and (39) can be reformulated as a two-step implicit FDM procedure of the form:

$$\tilde{L}^{j+1}\boldsymbol{u}_{j+1} = \tilde{E}^{j}\boldsymbol{u}_{j} + 2\boldsymbol{v}_{j} + \tilde{\boldsymbol{b}}^{j}, \tag{40}$$

$$\boldsymbol{v}_{j+1} = \left[\left(1+\frac{2}{\Delta t}\right)I + \tilde{W}\right]\boldsymbol{u}_{j+1} + \left[\left(1-\frac{2}{\Delta t}\right)I + \tilde{W}\right]\boldsymbol{u}_{j} - \boldsymbol{v}_{j}, \tag{41}$$

where:

$$\boldsymbol{u}_j = \big(u_{0,j},\ldots,u_{M,j}\big)^{\mathrm{T}}, \quad \boldsymbol{v}_j = \big(v_{0,j},\ldots,v_{M,j}\big)^{\mathrm{T}}, \quad \tilde{W} = \mathrm{diag}(w_0,\ldots,w_M),$$
I is the $(M+1)\times(M+1)$ identity matrix,

$$\tilde{L}^{j+1} = \begin{pmatrix} B_0+\lambda_1^{j+1} & -2A & 0 & \ldots & 0 & 0 & 0 \\ -A & B_1 & -A & \ldots & 0 & 0 & 0 \\ \vdots & \vdots & \vdots & \ddots & \vdots & \vdots & \vdots \\ 0 & 0 & 0 & \ldots & -A & B_{M-1} & -A \\ 0 & 0 & 0 & \ldots & 0 & -2A & B_M+\lambda_2^{j+1} \end{pmatrix},$$

$$\tilde{E}^{j} = \begin{pmatrix} C_0-\lambda_1^{j} & 2A & 0 & \ldots & 0 & 0 & 0 \\ A & C_1 & A & \ldots & 0 & 0 & 0 \\ \vdots & \vdots & \vdots & \ddots & \vdots & \vdots & \vdots \\ 0 & 0 & 0 & \ldots & A & C_{M-1} & A \\ 0 & 0 & 0 & \ldots & 0 & 2A & C_M-\lambda_2^{j} \end{pmatrix},$$

$$\tilde{\boldsymbol{b}}^{j} = \begin{pmatrix} \frac{\Delta t}{2}\big(f_{0,j}+f_{0,j+1}\big) + 2A\Delta x\Big(h_0^{j+1}u_{\infty,0}^{j+1} + h_0^{j}u_{\infty,0}^{j}\Big) \\ \frac{\Delta t}{2}\big(f_{1,j}+f_{1,j+1}\big) \\ \vdots \\ \frac{\Delta t}{2}\big(f_{M-1,j}+f_{M-1,j+1}\big) \\ \frac{\Delta t}{2}\big(f_{M,j}+f_{M,j+1}\big) + 2A\Delta x\Big(h_{\mathrm{L}}^{j+1}u_{\infty,\mathrm{L}}^{j+1} + h_{\mathrm{L}}^{j}u_{\infty,\mathrm{L}}^{j}\Big) \end{pmatrix},$$

where $\lambda_1^j = 2A\Delta x h_0^j$ and $\lambda_2^j = 2A\Delta x h_{\mathrm{L}}^j$ for $j = \overline{0,(N-1)}$.

We next consider a numerical example to verify the convergence and accuracy of the proposed FDM scheme.

3.1 Verification example

We consider the direct problem (14)–(16) with $\mathrm{L} = \mathrm{t_f} = 1$ and the following input data:

$$u(x,0) = \phi(x) = x + \sin(\pi x) + 5, \quad \frac{\partial u}{\partial t}(x,0) = \psi(x) = 1, \tag{42}$$

$$h_0(t) = h_{\mathrm{L}}(t) = 1, \quad u_{\infty,0}(t) = t - \pi + 4, \quad u_{\infty,\mathrm{L}}(t) = t - \pi + 7, \tag{43}$$

$$f(x,t) = x + (x+1)\big(t + x + \sin(\pi x) + 5\big) + \pi^2 \sin(\pi x) + 2, \tag{44}$$

and

$$w(x) = 1 + x. \tag{45}$$

Then, the exact solution is given by

$$u(x,t) = x + t + 5 + \sin(\pi x). \tag{46}$$

The root mean square error ($rmse$) given by

$$rmse\big(u_{\mathrm{t_f}}\big) = \sqrt{\frac{1}{M+1}\sum_{i=0}^{M}\Big[u_{\mathrm{t_f}}^{\mathrm{numerical}}(x_i) - u_{\mathrm{t_f}}^{\mathrm{exact}}(x_i)\Big]^2} \tag{47}$$

was obtained as $rmse(u_{\mathrm{t_f}}) \in \{0.0354, 0.0083, 0.002\}$ for $M = N \in \{5, 10, 20\}$, respectively, indicating that the order of convergence of the FDM is two.

In the next section, the inverse problem of identifying the space-dependent blood perfusion coefficient $w(x)$ alongside the temperature $u(x,t)$ in the inverse problem (14)–(17) is recast as a constrained minimization problem and a procedure based on the MATLAB built-in routine *lsqnonlin* is described for the solution of such a minimization problem.

4. Numerical solution of inverse problem

In this section, we wish to obtain accurate and stable reconstructions of the unknown blood perfusion coefficient $w(x)$ and the temperature $u(x,t)$ satisfying the inverse problem (14)–(17) reformulated as minimizing the regularized objective function

$$G(w) \coloneqq ||u(\cdot, \mathrm{t_f}) - u_{\mathrm{t_f}}(\cdot)||^2 + \lambda ||w(\cdot)||^2, \tag{48}$$

where u solves the direct problem (14)–(16) for a given element $w(x)$, $\lambda \geq 0$ is a regularization parameter to be prescribed and the norm is the $L^2[0, \mathrm{L}]$-norm.

The discrete form of (48) reads as

$$G(\boldsymbol{w}) = \sum_{i=0}^{M}\big[u(x_i, \mathrm{t_f}) - u_{\mathrm{t_f}}(x_i)\big]^2 + \lambda \sum_{i=0}^{M} w_i^2, \tag{49}$$

where $\boldsymbol{w} = (w_i)_{i=\overline{0,M}} \in \mathbb{R}_+^{M+1}$. The minimization of the objective function (49) is performed using the MATLAB optimization toolbox routine *lsqnonlin*, which does not require supplying by the user the gradient of the objective function (49), [23]. This routine attempts to find the minimum of a sum of squares by starting from an arbitrary initial guess $\boldsymbol{w}^{(0)}$ for $\boldsymbol{w}$. This routine is compiled with the following parameters:

- Algorithm is the Trust-Region-Reflective (TRR) minimization, [10].
- Maximum number of iterations = 400.
- Maximum number of objective function evaluations = $10^2 \times$ (number of variables).

- Termination tolerance on the function value = 10^{-20}.
- Solution tolerance = 10^{-20}.
- Lower and upper simple bounds on the unknowns are 10^{-10} (very small positive number) and 10^{3} (large positive number), respectively.

The inverse problem (14)–(17) is solved subject to both exact and noisy final time temperature measurements (17). The noisy data are numerically simulated as follows:

$$u^{\epsilon}_{\mathrm{t_f}}(x_i) = u_{\mathrm{t_f}}(x_i) + \epsilon_i, \quad i = \overline{0, M}, \tag{50}$$

where ϵ_i are random variables generated from a Gaussian normal distribution with mean zero and standard deviation σ given by

$$\sigma = p \times \max_{x\in[0,\mathrm{L}]} |u_{\mathrm{t_f}}(x)|, \tag{51}$$

where p is the percentage of noise. We use the MATLAB function $normrnd(0, \sigma, M+1)$ to generate the random variables $\boldsymbol{\epsilon} = (\epsilon_i)_{i=\overline{0,M}}$. In the case of noisy data (50), we replace $u_{\mathrm{t_f}}(x_i)$ by $u^{\epsilon}_{\mathrm{t_f}}(x_i)$ in (49).

The convergence, accuracy and stability of the procedure just described are tested for three numerical benchmark examples in which the blood perfusion coefficient exhibits different behaviours such as smooth, piecewise smooth or discontinuous. Moreover, the reconstruction of the blood perfusion rate of a real-world laser-irradiated biological tissue is performed.

5. Numerical results and discussion

This section assesses the convergence, accuracy, and stability of the minimization procedure described in the previous section. We test for a: (i) smooth (Example 1), (ii) piecewise smooth (Example 2) and (iii) discontinuous (Example 3) space-dependent blood perfusion $w(x)$. Furthermore, we consider retrieving a dimensional blood perfusion rate of a biological tissue irradiated by laser (Example 4). The root mean square error ($rmse$) is utilized to evaluate the accuracy of the reconstructed perfusion coefficient $w(x)$, as follows:

$$rmse(w) = \sqrt{\frac{\mathrm{L}}{M+1}\sum_{i=0}^{M}\left[w^{\mathrm{numerical}}(x_i) - w^{\mathrm{exact}}(x_i)\right]^2}. \tag{52}$$

In the first three benchmark numerical examples presented below we take, for simplicity, $\mathrm{t_f} = \mathrm{L} = 1$. We also take $M = N = 40$ in the inverse calculations.

5.1 Example 1 (smooth coefficient)

We consider the inverse problem (14)–(17) with a linear and smooth unknown blood perfusion coefficient $w(x)$ with the input data (42)–(44) and

$$u_{\mathrm{t_f}}(x) = x + \sin(\pi x) + 6. \tag{53}$$

The analytical solution with the above input data is given by (45) and (46). We take the initial guess for $w(x)$ as the parabola given by

$$w^0(x) = x^2 + 1, \quad x \in [0, \mathrm{L}], \tag{54}$$

which is reasonably different from the true solution (45). In general, other initial guesses produced similar results but, of course, since the inverse problem is non-linear the objective functional (49) is non-convex and the iterative process of minimization requires a good initial guess; otherwise one can get stuck in a local minimum.

First of all, we start the investigation of identifying the space-dependent blood perfusion coefficient $w(x)$, where there is no noise in the final time temperature measurement (53), i.e. $p = 0$ in (51). The unregularized (i.e. with $\lambda = 0$) objective function (49), as a function of the number of iterations, is displayed in Figure 1(a), showing a rapid monotonic decreasing convergence to a low value of $\mathcal{O}(10^{-25})$ in 7 iterations. The corresponding numerical retrieval of $w(x)$ is presented in Figure 1(b) in comparison with the exact solution (45), where we accomplish a small $rmse(w) = 2.4 \times 10^{-3}$. From this figure, it can be seen that an accurate and stable numerical solution is obtained.

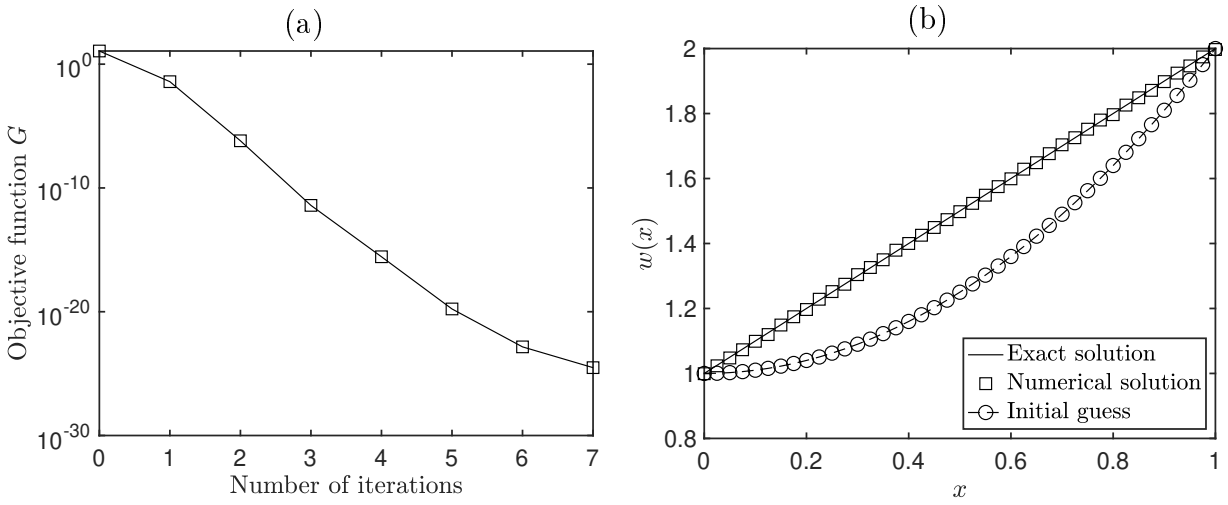

Figure 1: (a) The objective function (49), as a function of the number of iterations, and (b) the perfusion coefficient $w(x)$, with no noise and no regularization, for Example 1.

Next, the stability of the numerical solution is investigated with respect to noise in the data (50). We add various levels of noise $p \in \{0.01, 0.1\}\%$ to the input data (17), via (50) and (51). Figures 2 and 3 illustrate the recovered function $w(x)$, without and with regularization. From Figures 2(a) and 3(a), it can be seen that the numerical solutions for $w(x)$ with no regularization possess some oscillations with $rmse(w) = 0.5151$ for $p = 0.01\%$ and $rmse(w) = 0.8802$ for $p = 0.1\%$. This is expected since the inverse problem (14)–(17) is ill-posed and sensitive to small perturbations into the measurement (17). Hence, regularization is necessary to store the stability of the solution. Throughout this section, we choose the Tikhonov regularization parameter based on trial and error. That is, we start

with a small value of λ and then gradually increase it until any high oscillations disappear. By doing so, we conclude that the choices of $\lambda = 10^{-5}$ for $p = 0.01\%$; see Figure 2(b), and $\lambda = 10^{-3}$ for $p = 0.1\%$; see Figure 3(b), provide accurate and stable numerical solutions for the space-dependent blood perfusion coefficient $w(x)$, where we accomplish small $rmse(w) \in \{0.0956, 0.1829\}$ for $p \in \{0.01, 0.1\}\%$, respectively. The corresponding numerical solution for the temperature $u(x,t)$ is depicted in Figure 4 alongside the exact solution (46) and the absolute errors between them. From this figure it can be seen that good agreement between the exact and numerical solutions for $u(x,t)$ is achieved. From Figures 1(b), 2(b), 3(b), 4 and Table 1, it can be concluded that convergence of the numerical solutions for the pair of functions $\big(w(x), u(x,t)\big)$ with respect to decreasing the percentage of noise p from 0.1% to 0.01% and then to zero has been accomplished.

Table 1: The $rmse(w)$ defined by (52), the minimum value of (49) and the number of iterations for $p \in \{0, 0.01, 0.1\}\%$ noise, and without and with regularization, for Example 1.

p	λ	$rmse(w)$	Minimum value of (49)	Iter
0	0	2.4×10^{-3}	3.1×10^{-25}	7
0.01%	0	0.5151	1.1×10^{-6}	50
	10^{-6}	0.1456	9.8×10^{-5}	40
	10^{-5}	0.0956	9.6×10^{-4}	38
	10^{-4}	0.1049	9.5×10^{-3}	44
	10^{-3}	0.1405	9.4×10^{-2}	36
0.1%	0	0.8802	3.3×10^{-4}	88
	10^{-4}	0.2722	1.1×10^{-2}	41
	10^{-3}	0.1829	9.7×10^{-2}	39
	10^{-2}	0.1885	9.4×10^{-1}	97
	10^{-1}	0.2411	9.1439	97

5.2 Example 2 (piecewise smooth coefficient)

The previous example has considered retrieving a simple linear space variation of the perfusion coefficient (45). In this example, we investigate the numerical algorithm for estimating a less smooth coefficient given by (56) below. We take the input data given by (42), (43), (53) and

$$f(x,t) = \left|x - \frac{1}{2}\right| + \pi^2 \sin(\pi x) + \left(\left|x - \frac{1}{2}\right| + \frac{1}{2}\right)\big(t + x + \sin(\pi x) + 5\big) + \frac{3}{2}. \tag{55}$$

Then, the analytical solution with this input data is given by (46) for the temperature $u(x,t)$ and

$$w(x) = \left|x - \frac{1}{2}\right| + \frac{1}{2}, \tag{56}$$

for the blood perfusion coefficient. The initial guess for the unknown function $w(x)$ in this example is taken as 1, namely,

$$w^0(x) = 1, \quad x \in [0, \mathrm{L}]. \tag{57}$$

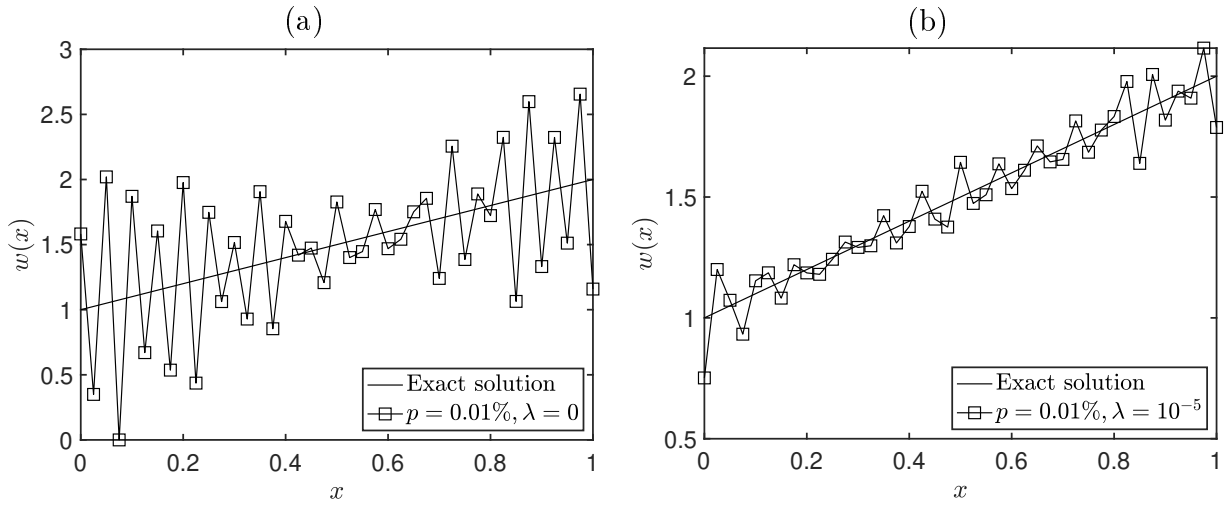

Figure 2: The exact (45) and numerical perfusion coefficient $w(x)$, for $p = 0.01\%$ noise and (a) $\lambda = 0$ (i.e. without regularization) and (b) $\lambda = 10^{-5}$ (i.e. with regularization), for Example 1.

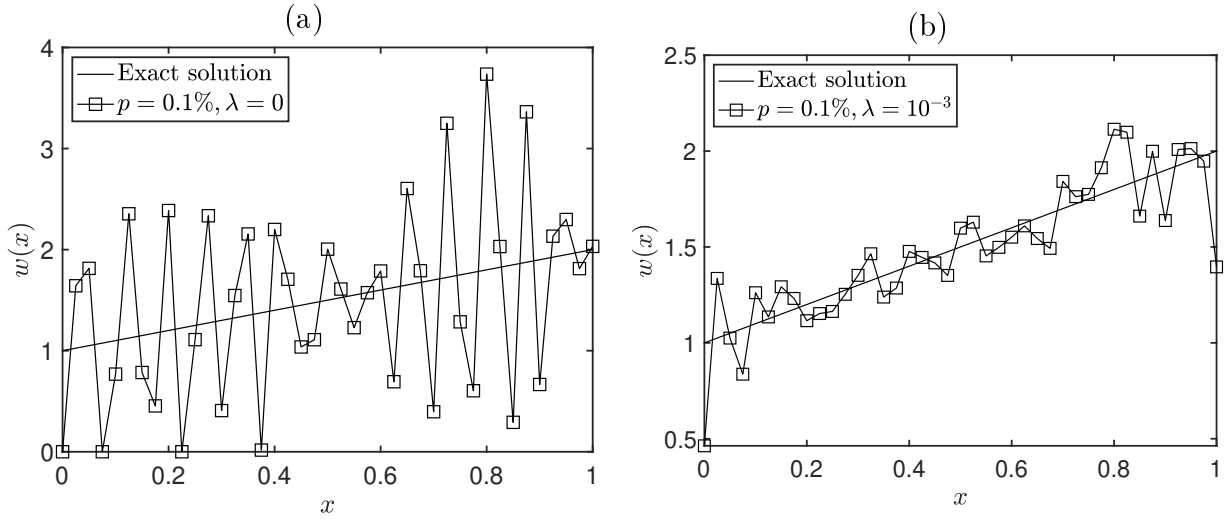

Figure 3: The exact (45) and numerical perfusion coefficient $w(x)$, for $p = 0.1\%$ noise and (a) $\lambda = 0$ (i.e. without regularization) and (b) $\lambda = 10^{-3}$ (i.e. with regularization), for Example 1.

As previously carried out in Example 1, we begin the examination of estimating the space-dependent perfusion coefficient $w(x)$ in the case of noise-free input data, i.e. $p = 0$ in (51). The unregularized (i.e. with $\lambda = 0$) objective function (49), as a function of the number of iterations, is plotted in Figure 5(a). From this figure it can be observed that a rapid monotonic decreasing convergence to a low value of $\mathcal{O}(10^{-25})$ is achieved in 10 iterations. Figure 5(b) depicts the numerical reconstruction of $w(x)$ alongside the exact solution (56), where we achieve a small $rmse(w) = 1.9 \times 10^{-3}$. From this figure it can be observed, as in Example 1, that an accurate and stable numerical solution for $w(x)$ is obtained.

(a)

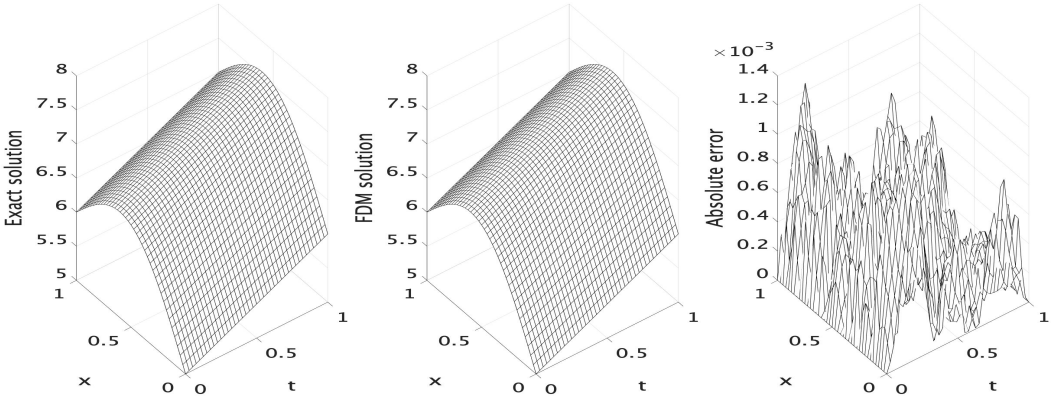

(b)

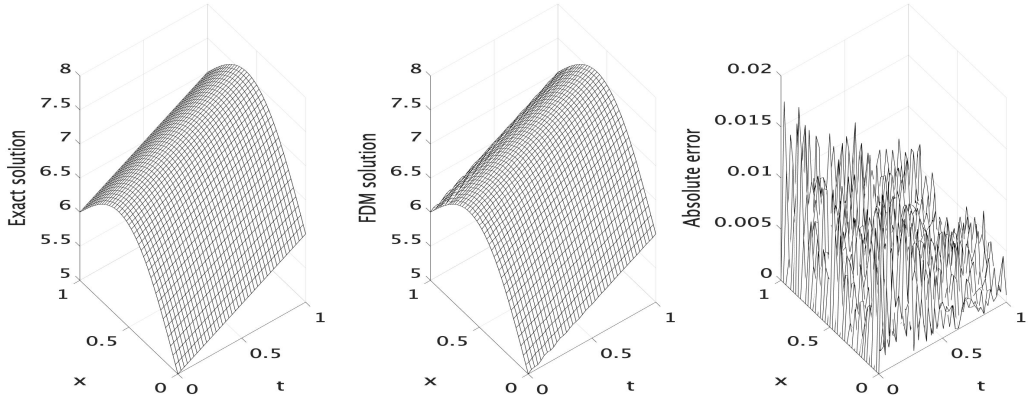

(c)

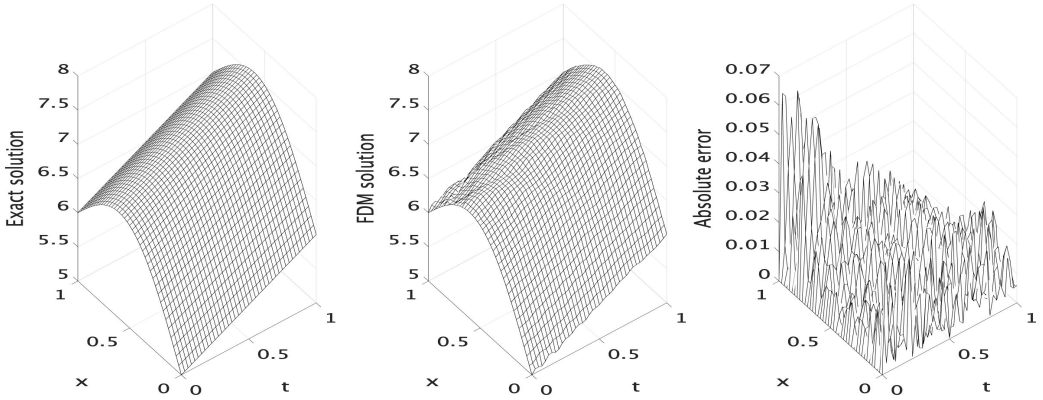

Figure 4: The analytical (46) and numerical solutions for the temperature $u(x,t)$, with (a) $p = 0$ and $\lambda = 0$ (i.e. with no noise and no regularization), (b) $p = 0.01\%$ noise and $\lambda = 10^{-5}$, and (c) $p = 0.1\%$ noise and $\lambda = 10^{-3}$, for Example 1. The absolute errors between them are also included.

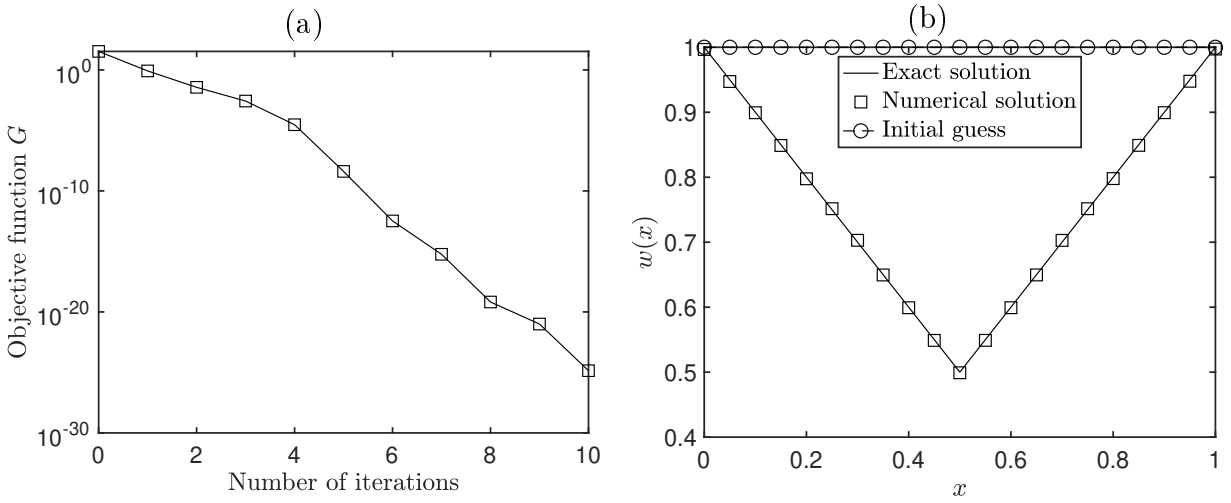

Figure 5: (a) The objective function (49), as a function of the number of iterations, and (b) the perfusion coefficient $w(x)$, with no noise and no regularization, for Example 2.

Next, we include $p \in \{0.01, 0.1\}\%$ noise in $u_{\mathrm{t_f}}(x)$ given by (53), using (50) and (51), to assess the stability of the numerical solution. The estimated perfusion coefficient $w(x)$ is presented in Figures 6 and 7, without and with regularization. As in Example 1, high oscillatory and inaccurate solutions for $w(x)$ are obtained with $rmse(w) = 0.5184$ for $p = 0.01\%$ and $rmse(w) = 0.5682$ for $p = 0.1\%$, when regularization is not implemented; see Figures 6(a) and 7(a). Therefore, regularization is required to recover the stability of the solution. By trial and error we conclude that the choices of $\lambda = 10^{-5}$ for $p = 0.01\%$; see Figure 6(b), and $\lambda = 10^{-2}$ for $p = 0.1\%$; see Figure 7(b), provide accurate and stable numerical solutions for $w(x)$, where we obtain small $rmse(w) \in \{0.0721, 0.1329\}$ for $p \in \{0.01, 0.1\}\%$, respectively. The corresponding numerical solutions for the temperature $u(x,t)$ are shown in Figure 8 in comparison with the exact solution (46) and the absolute errors between them. From this figure, it can be observed that good agreement between the exact and numerical solutions is accomplished. From Figures 5(b), 6(b), 7(b), 8 and Table 2, it can be concluded, as in Example 1, that the numerical solutions become closer to the exact solution as p decreases from 0.1% to 0.01% and then to zero.

5.3 Example 3 (discontinuous coefficient)

The previous two examples possessed an analytical solution available for the pair of functions $\big(w(x), u(x,t)\big)$. In this example, we examine the proposed inversion method for reconstructing a discontinuous coefficient given by (60) associated with an example for which an analytical solution for $u(x,t)$ is not available. We take (44) for the source $f(x,t)$ and the following input data:

$$u(x,0) = \phi(x) = 0, \quad \frac{\partial u}{\partial t}(x,0) = \psi(x) = 0, \tag{58}$$

$$h_0(t) = h_{\mathrm{L}}(t) = 0, \quad u_{\infty,0}(t) = u_{\infty,\mathrm{L}}(t) = 0. \tag{59}$$

With (59), the boundary conditions (16) become adiabatic. As for the blood perfusion

Table 2: The $rmse(w)$ defined by (52), the minimum value of (49) and the number of iterations for $p \in \{0, 0.01, 0.1\}\%$ noise, and without and with regularization, for Example 2.

p	λ	$rmse(w)$	Minimum value of (49)	Iter
0	0	1.9×10^{-3}	1.4×10^{-25}	10
0.01%	0	0.5184	7.9×10^{-7}	63
	10^{-6}	0.1095	2.6×10^{-5}	45
	10^{-5}	0.0721	2.4×10^{-4}	52
	10^{-4}	0.0725	2.4×10^{-3}	42
	10^{-3}	0.0891	2.4×10^{-2}	40
0.1%	0	0.5682	8.1×10^{-5}	58
	10^{-4}	0.2547	2.8×10^{-3}	46
	10^{-3}	0.1453	2.5×10^{-2}	47
	10^{-2}	0.1329	2.3×10^{-1}	97
	10^{-1}	0.2005	2.2102	97

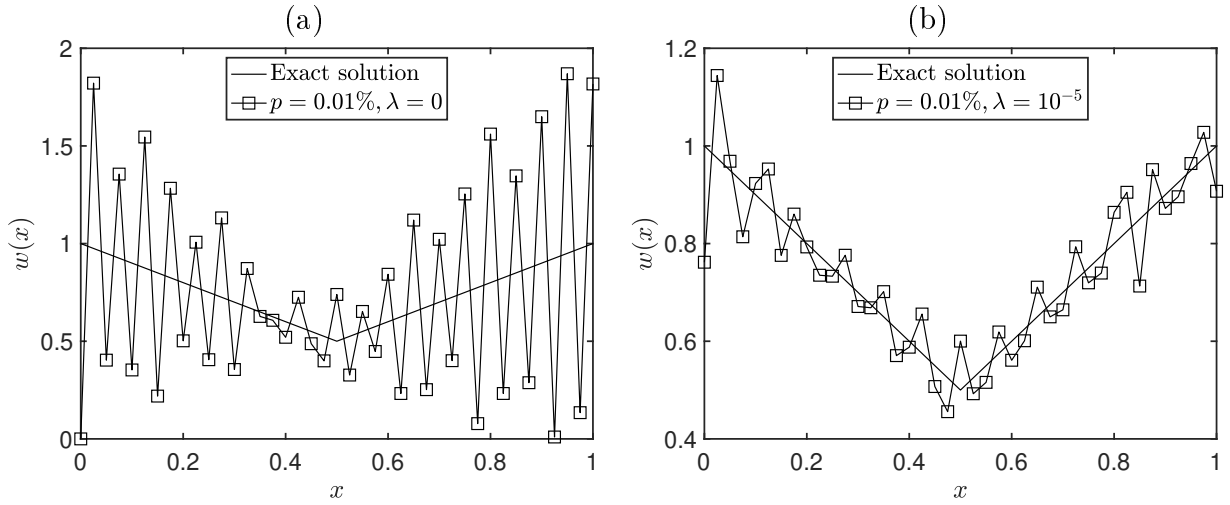

Figure 6: The exact (56) and numerical perfusion coefficient $w(x)$, for $p = 0.01\%$ noise and (a) $\lambda = 0$ (i.e. without regularization) and (b) $\lambda = 10^{-5}$ (i.e. with regularization), for Example 2.

coefficient $w(x)$, we take

$$w(x) = \begin{cases} 1, & 0.25 \le x \le 0.75, \\ 0, & \text{otherwise}, \end{cases} \tag{60}$$

which represents a discontinuous piecewise constant function. In the absence of an analytical solution for the temperature $u(x,t)$ being available, we generate the input data (17) numerically by solving first the direct problem (14)–(16), using the FDM described in Section 3, with the input (44) and (58)–(60), where the blood perfusion coefficient (60) is assumed to be known. The numerical results for $u_{\mathrm{t_f}}(x)$ in equation (17) are shown in Figure 9, for various

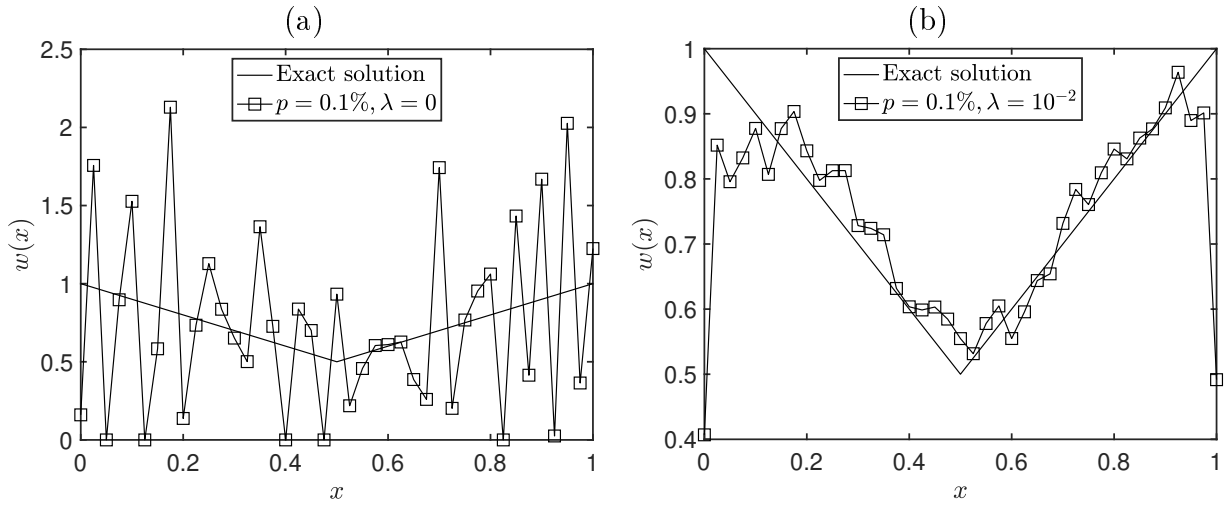

Figure 7: The exact (56) and numerical perfusion coefficient $w(x)$, for $p = 0.1\%$ noise and (a) $\lambda = 0$ (i.e. without regularization) and (b) $\lambda = 10^{-2}$ (i.e. with regularization), for Example 2.

mesh sizes $M = N \in \{20, 40, 60\}$, showing that convergent results have been achieved.

We consider half of the data for $u_{\mathrm{t_f}}(x)$ obtained by solving the direct problem with $M = N = 80$ as our input data (17) and then solve the inverse problem with a coarser mesh of $M = N = 40$ to avoid committing an inverse crime. We take the initial guess for the unknown perfusion coefficient $w(x)$ as

$$w^0(x) = 0.4, \quad x \in [0, \mathrm{L}]. \tag{61}$$

Analogous quantities and conclusions to Figures 1–3 and Table 1 of Example 1 and Figures 5–7 and Table 2 of Example 2 are presented and obtained in Figures 10–12 and Table 3 of Example 3.

The examples considered so far have been benchmark test examples to demonstrate the numerical procedure proposed for reconstructing test functions of decreasing smoothness. The following example illustrates the inversion algorithm for retrieving a blood perfusion rate w_b associated with a physical situation of an irradiated biological tissue.

5.4 Example 4 (irradiated biological tissue)

Unlike the previous examples that considered identifying fabricated perfusion coefficients (smooth, piecewise smooth and discontinuous), in this final example we consider recovering the blood perfusion rate w_b in the governing equation (2)–(5) associated with a one-dimensional, one-layered biological tissue. We assume that the biological tissue undergoes laser irradiation of the form, [34],

$$Q_e(x) = \rho_{\mathrm{t}} \kappa \Lambda_0 e^{g(x-0.01)}, \quad x \in [0, L], \tag{62}$$

where κ [kg^{-1}] and g [m^{-1}] are the antenna constants, and Λ_0 [W] is the transmitted power.

The initial and boundary conditions taken from [1] and [12], respectively, read as:

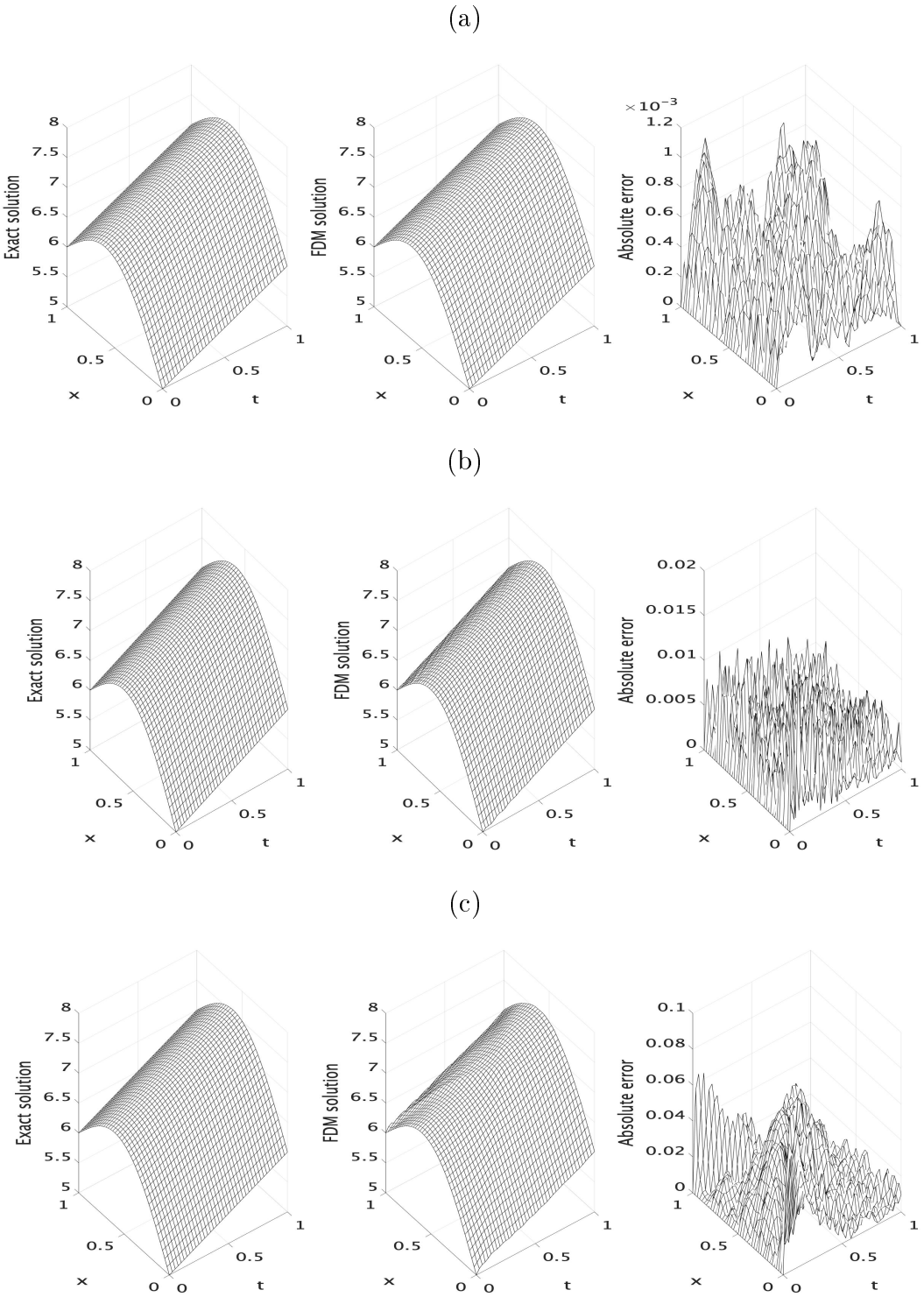

Figure 8: The analytical (46) and numerical solutions for the temperature $u(x,t)$, with (a) $p = 0$ and $\lambda = 0$ (i.e. with no noise and no regularization), (b) $p = 0.01\%$ noise and $\lambda = 10^{-5}$, and (c) $p = 0.1\%$ noise and $\lambda = 10^{-2}$, for Example 2. The absolute errors between them are also included.

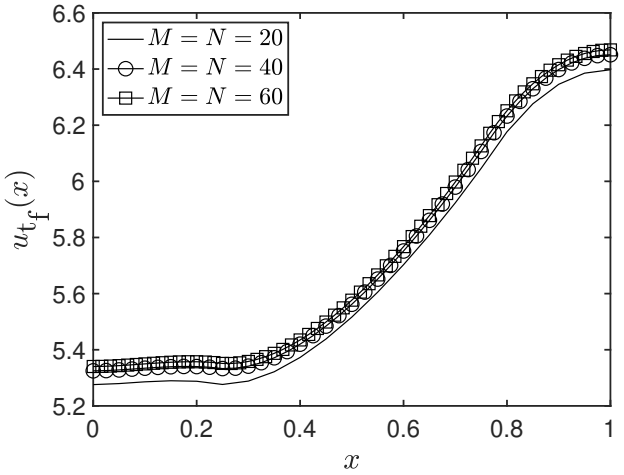

Figure 9: The numerical solutions for $u_{t_f}(x)$ of the direct problem of Example 3 with various mesh sizes $M = N \in \{20, 40, 60\}$.

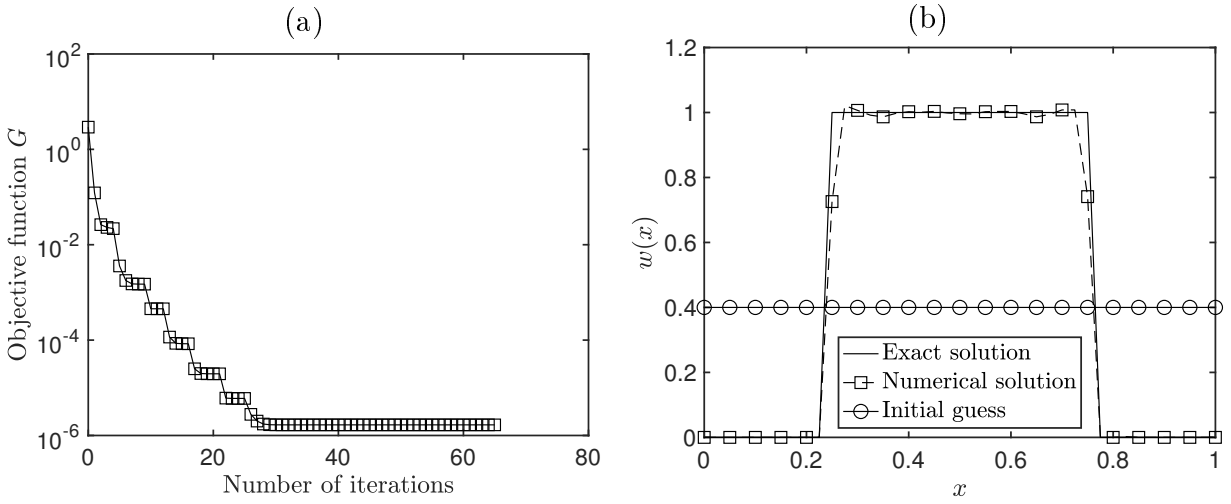

Figure 10: (a) The objective function (49), as a function of the number of iterations, and (b) the perfusion coefficient $w(x)$, with no noise and no regularization, for Example 3.

$T|_{t=0} = \phi = 37$ °C, $T_t|_{t=0} = \psi = 0$ and $h_0 = h_L = T_{\infty,0} = T_{\infty,L} = 0$. We also take $t_f = 100$ s and $L = 0.04$ m from [18]. The thermo-physical properties of the tissue are taken as the reference values presented in Table 4. The values of the parameters in the source (62) are considered as: $\kappa = 12.5$ kg^{-1}, $g = -127$ m^{-1} and $\Lambda_0 = 5$ W, [34].

The above dimensional quantities transform, via (13), into the following dimensionless input data:

$$\mathrm{L} = 25.2666,\ \mathrm{t_f} = 5,\ w(x) = 0.8,\ u(x,0) = \phi(x) = 0, \tag{63}$$

$$\frac{\partial u}{\partial t}(x,0) = \psi(x) = 0,\ h_0(t) = h_{\mathrm{L}}(t) = 0,\ u_{\infty,0}(t) = u_{\infty,\mathrm{L}}(t) = 0, \tag{64}$$

$$f(x,t) = 0.0089e^{-0.2011x+1.27} + 0.0046. \tag{65}$$

Table 3: The $rmse(w)$ defined by (52), the minimum value of (49) and the number of iterations for $p \in \{0, 0.01, 0.1\}\%$ noise, and without and with regularization, for Example 3.

p	λ	$rmse(w)$	Minimum value of (49)	Iter
0	0	0.0592	1.7×10^{-6}	65
0.01%	0	0.1162	1.5×10^{-5}	59
	10^{-6}	0.1089	3.5×10^{-5}	62
	10^{-5}	0.0849	2.2×10^{-4}	63
	10^{-4}	0.1007	1.9×10^{-3}	52
	10^{-3}	0.1405	1.9×10^{-2}	56
0.1%	0	0.6854	9.1×10^{-4}	83
	10^{-4}	0.1685	3.3×10^{-3}	59
	10^{-3}	0.1498	2.1×10^{-2}	52
	10^{-2}	0.1913	1.8×10^{-1}	49
	10^{-1}	0.2836	1.4815	97

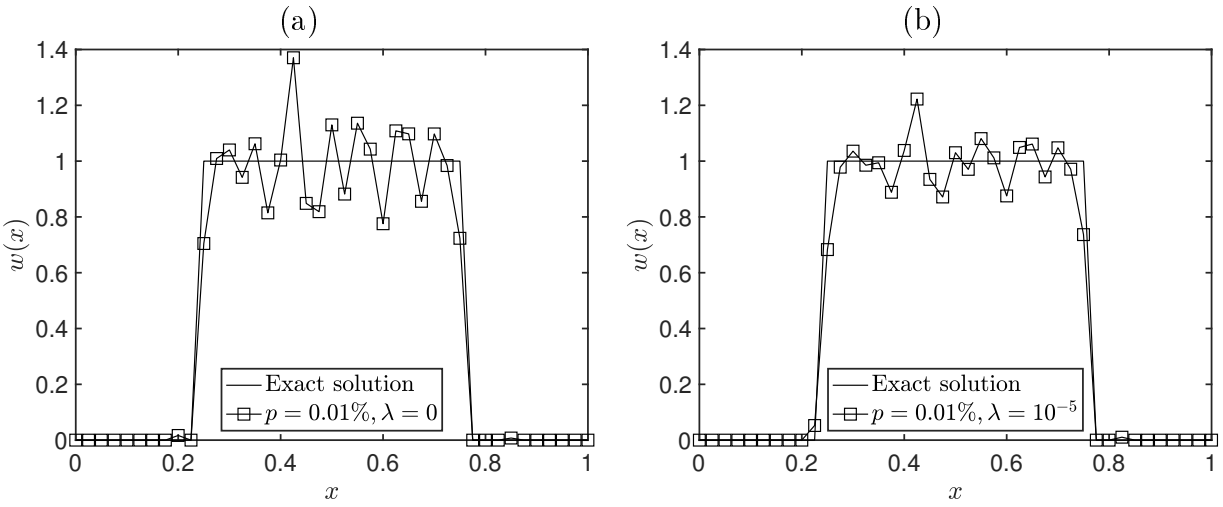

Figure 11: The exact (60) and numerical perfusion coefficient $w(x)$, for $p = 0.01\%$ noise and (a) $\lambda = 0$ (i.e. without regularization) and (b) $\lambda = 10^{-5}$ (i.e. with regularization), for Example 3.

We wish to recover the perfusion coefficient $w(x) = 0.8$ for $x \in [0, 25.2666]$ and the tissue temperature $u(x,t)$, allowing us to obtain, via (13), the dimensional quantities $w_b(x)$ and $T(x,t)$. This knowledge is required, for instance, in computing the Arrhenius thermal damage, [1, 25].

In the absence of an analytical solution for the temperature $u(x,t)$ being available, we generate the input data (17) numerically by solving first the direct problem (14)–(16), using the FDM described in Section 3, with the input data (63)–(65), where the blood perfusion coefficient $w(x)$ is assumed known. The numerical solutions for $u_{\mathrm{t_f}}(x)$ in equation (17) are depicted in Figure 13, for various mesh sizes $M = N \in \{5, 10, 15\}$. From this figure it can

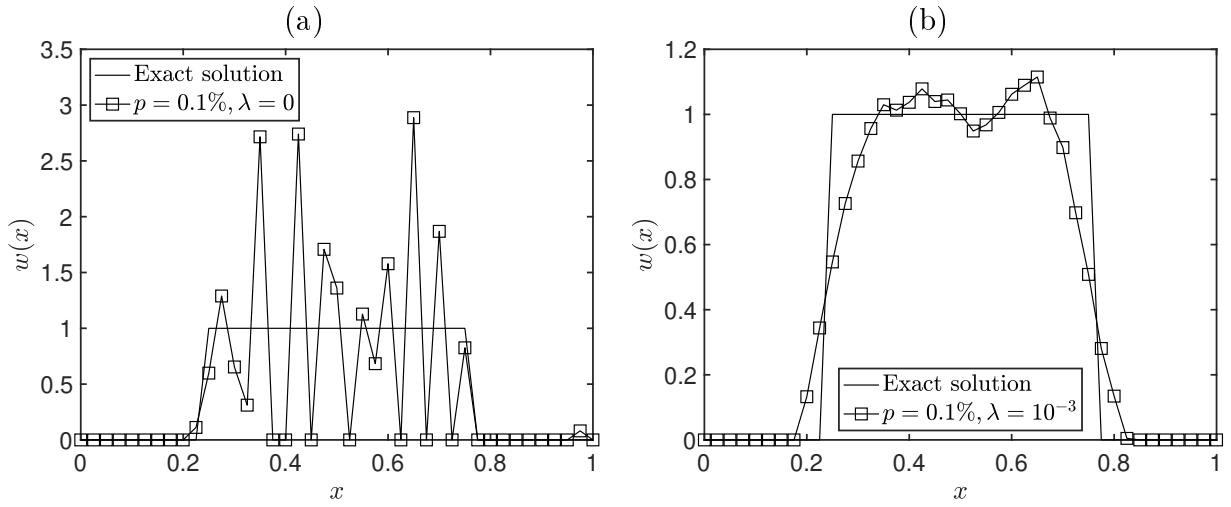

Figure 12: The exact (60) and numerical perfusion coefficient $w(x)$, for $p = 0.1\%$ noise and (a) $\lambda = 0$ (i.e. without regularization) and (b) $\lambda = 10^{-3}$ (i.e. with regularization) for Example 3.

Table 4: Thermo-physical properties of a typical skin tissue.

Symbol	Value	Unit	Ref.
$\rho_{\mathrm{t}}, \rho_b$	1050	$\mathrm{kg/m^3}$	[2]
c_{t}, c_b	3800	J/(kg °C)	[2]
k	0.5	W/(m °C)	[2]
w_b	0.04	$\mathrm{s^{-1}}$	[2]
T_a	37	°C	[2]
τ	20	s	[26]
Q_m	33800	$\mathrm{W/m^3}$	[18]

be concluded that convergent numerical solutions have been obtained.

We consider half of the data for $u_{\mathrm{t_f}}(x)$ obtained by solving the direct problem with $M = N = 80$ as our input data (17) and then solve the inverse problem with a coarser mesh of $M = N = 40$ to avoid committing an inverse crime. In this example, we take the initial guess (61). Figure 14 depicts the unregularized (i.e. with $\lambda = 0$) objective function (49), as a function of the number of iterations, for exact (i.e. $p = 0$) and noisy (with $p = 0.1\%$ noise) data. From this figure, a rapid monotonic decreasing convergence to low values of $\mathcal{O}(10^{-31})$ in only 6 iterations is observed.

Figure 15 shows the corresponding numerical solutions for the space-wise perfusion function $w_b(x)$. From this figure, it can be seen that accurate and stable numerical identifications are obtained from both exact and noisy measurements. No regularization was found necessary for such a small amount of noise in the data, but, nevertheless, this needs to be enforced for higher levels of noise.

6. Conclusions

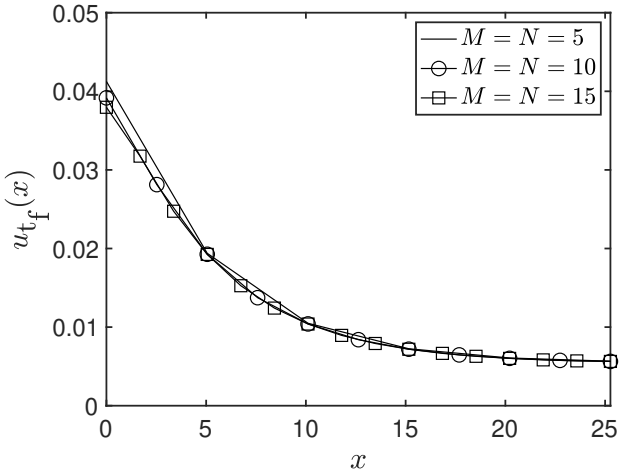

Figure 13: The numerical solutions for $u_{t_f}(x)$ of the direct problem of Example 4 with various mesh sizes $M = N \in \{5, 10, 15\}$.

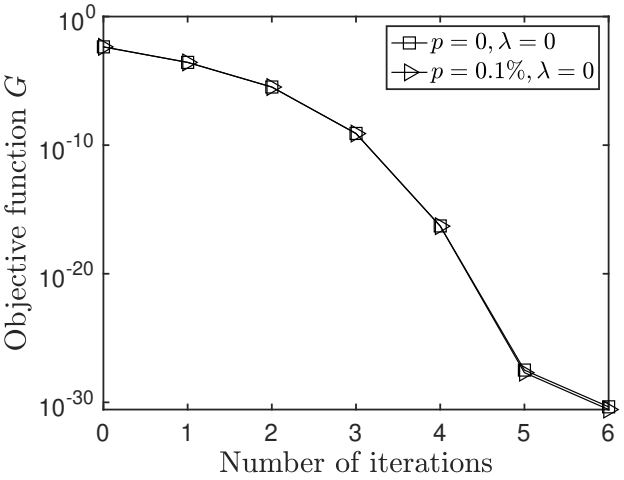

Figure 14: The objective function (49), as a function of the number of iterations, with no noise (i.e. with $p = 0$) and $p = 0.1\%$ noise, and no regularization, for Example 4.

The reconstruction of the space-dependent perfusion coefficient and the temperature in the thermal-wave model of bio-heat transfer from final time temperature measurement has been investigated. For the numerical discretization, an unconditionally stable FDM based on the Crank-Nicolson scheme has been used as a direct solver. This has been combined with a constrained regularized minimization problem. The resulting objective functional, penalized by a Tikhonov regularization term to restore the stability of the solution, has been minimized iteratively using the MATLAB optimization toolbox routine *lsqnonlin*. Accurate and stable numerical solutions for the unknown perfusion coefficient and the temperature, from both exact and noisy data, have been successfully achieved using the proposed computational method which has been verified for three benchmark numerical examples. Moreover, a dimensional blood perfusion rate of a biological tissue subjected to an external source of laser irradiation has been successfully identified.

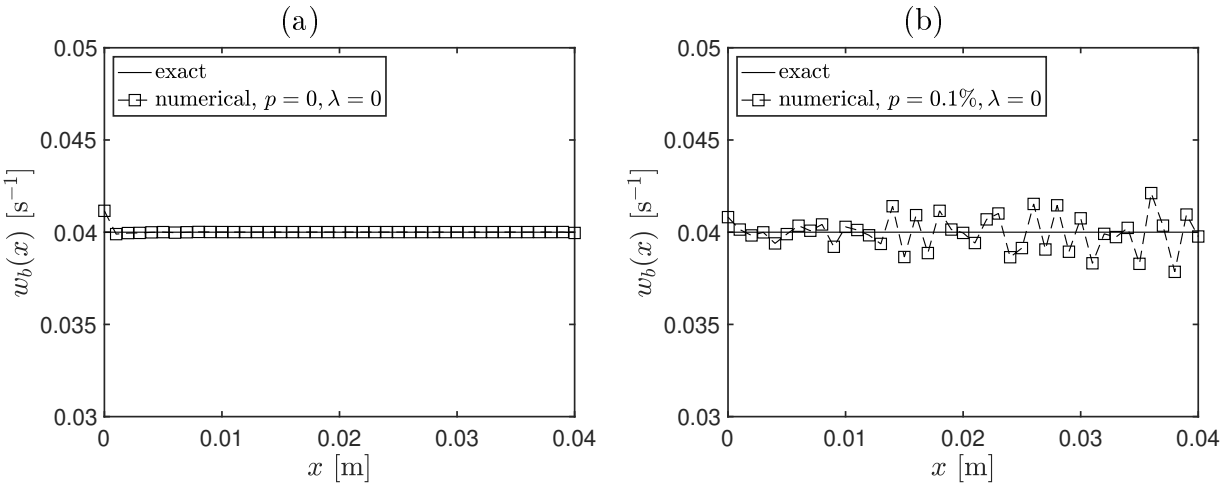

Figure 15: The retrieved coefficient $w_b(x)$, with (a) no noise (i.e. $p = 0$) and (b) $p = 0.1\%$ noise, and no regularization, for Example 4.

The analysis presented in this paper can be extended to more complex and potentially more accurate governing equations of bio-heat transfer, e.g. models of fractional-order or in integro-differential form. This extension will be undertaken in future work.

Declaration

Conflict of interest. All authors declare that they have no conflicts of interest.

References

[1] H. Ahmadikia, R. Fazlali, and A. Moradi. Analytical solution of the parabolic and hyperbolic heat transfer equations with constant and transient heat flux conditions on skin tissue. *International Communications in Heat and Mass Transfer*, 39(1):121–130, 2012.

[2] A. Alkhwaji, B. Vick, and T. Diller. New mathematical model to estimate tissue blood perfusion, thermal contact resistance and core temperature. *Journal of Biomechanical Engineering-Transactions of the ASME*, 134:081004, 2012.

[3] M. Alosaimi, D. Lesnic, and J. Niesen. Reconstruction of the thermal properties in a wave-type model of bio-heat transfer. *International Journal of Numerical Methods for Heat & Fluid Flow*, 30(12):5143–5167, 2020.

[4] M. Alosaimi, D. Lesnic, and J. Niesen. Determination of the thermo-physical properties of multi-layered biological tissues. *Applied Mathematical Modelling*, 99:228–242, 2021.

[5] M. Alosaimi, D. Lesnic, and J. Niesen. Identification of the thermo-physical properties

of a stratified tissue. Adiabatic hypodermic wall. *International Communications in Heat and Mass Transfer*, 126:105376, 2021.

[6] F. S. Bazán, L. Bedin, and L. S. Borges. Space-dependent perfusion coefficient estimation in a 2D bioheat transfer problem. *Computer Physics Communications*, 214:18–30, 2017.

[7] B. Bertman and D. J. Sandiford. Second sound in solid helium. *Scientific American*, 222(5):92–103, 1970.

[8] K. Cao and D. Lesnic. Reconstruction of the space-dependent perfusion coefficient from final time or time-average temperature measurements. *Journal of Computational and Applied Mathematics*, 337:150–165, 2018.

[9] C. Cattaneo. Sur une forme de l'equation de la chaleur eliminant la paradoxe d'une propagation instantantee. *Comptes Rendus de L'Académie Des Sciences*, 247:431–433, 1958.

[10] T. F. Coleman and Y. Li. An interior trust region approach for nonlinear minimization subject to bounds. *SIAM Journal on Optimization*, 6(2):418–445, 1996.

[11] W. Dai and R. Nassar. A finite difference scheme for solving the heat transport equation at the microscale. *Numerical Methods for Partial Differential Equations*, 15(6):697–708, 1999.

[12] J.-R. Ho, C.-P. Kuo, and W.-S. Jiaung. Study of heat transfer in multilayered structure within the framework of dual-phase-lag heat conduction model using lattice Boltzmann method. *International Journal of Heat and Mass Transfer*, 46(1):55–69, 2003.

[13] M. Huntul, D. Lesnic, and T. Johansson. Determination of an additive time-and space-dependent coefficient in the heat equation. *International Journal of Numerical Methods for Heat and Fluid Flow*, 28(6):1352–1373, 2018.

[14] S. O. Hussein, D. Lesnic, and M. Yamamoto. Reconstruction of space-dependent potential and/or damping coefficients in the wave equation. *Computers and Mathematics with Applications*, 74(6):1435–1454, 2017.

[15] O. Y. Imanuvilov and M. Yamamoto. Global Lipschitz stability in an inverse hyperbolic problem by interior observations. *Inverse Problems*, 17(4):717–728, 2001.

[16] V. Isakov. Inverse parabolic problems with the final overdetermination. *Communications on Pure and Applied Mathematics*, 44(2):185–209, 1991.

[17] A. Jalali, M.-B. Ayani, and M. Baghban. Simultaneous estimation of controllable parameters in a living tissue during thermal therapy. *Journal of Thermal Biology*, 45: 37–42, 2014.

[18] E. Kengne and A. Lakhssassi. Bioheat transfer problem for one-dimensional spherical biological tissues. *Mathematical Biosciences*, 269:1–9, 2015.

[19] D. Lesnic, S. O. Hussein, and B. T. Johansson. Inverse space-dependent force problems for the wave equation. *Journal of Computational and Applied Mathematics*, 306:10–39, 2016.

[20] J. Liu, Z. Ren, and C. Wang. Interpretation of living tissue's temperature oscillations by thermal wave theory. *Chinese Science Bulletin*, 40(17):1493–1495, 1995.

[21] J. Liu, X. Chen, and L. X. Xu. New thermal wave aspects on burn evaluation of skin subjected to instantaneous heating. *IEEE Transactions on Biomedical Engineering*, 46 (4):420–428, 1999.

[22] S. Liu and R. Triggiani. Global uniqueness and stability in determining the damping and potential coefficients of an inverse hyperbolic problem. *Nonlinear Analysis: Real World Applications*, 12(3):1562–1590, 2011.

[23] Mathworks. Documentation optimization toolbox-least squares (model fitting) algorithms. *available at: www.mathworks.com/help/toolbox/optim/ug/brnoybu.html*, 2012.

[24] K. Mitra, S. Kumar, A. Vedevarz, and M. Moallemi. Experimental evidence of hyperbolic heat conduction in processed meat. *Journal of Heat Transfer*, 117(3):568–573, 1995.

[25] A. Narasimhan and S. Sadasivam. Non-Fourier bio heat transfer modelling of thermal damage during retinal laser irradiation. *International Journal of Heat and Mass Transfer*, 60:591–597, 2013.

[26] Ş. Özen, S. Helhel, and O. Çerezci. Heat analysis of biological tissue exposed to microwave by using thermal wave model of bio-heat transfer (TWMBT). *Burns*, 34(1): 45–49, 2008.

[27] A. Pazy. *Semigroups of Linear Operators and Applications to Partial Differential Equations*. Springer-Verlag, 1983.

[28] H. H. Pennes. Analysis of tissue and arterial blood temperatures in the resting human forearm. *Journal of Applied Physiology*, 1(2):93–122, 1948.

[29] V. Peshkov. Second sound in helium II. *Soviet Physics JETP*, 11(3):580–584, 1960.

[30] A. Prilepko, D. Orlovsky, and I. Vasin. *Methods for Solving Inverse Problems in Mathematical Physics*. Marcel Dekker, Inc., 2000.

[31] A. Ramm. An inverse problem for the heat equation. *Journal of Mathematical Analysis and Applications*, 264(2):691–697, 2001.

[32] Z. P. Ren, J. Liu, C. C. Wang, and P. X. Jiang. Boundary element method (BEM) for solving normal or inverse bio-heat transfer problem of biological bodies with complex shape. *Journal of Thermal Science*, 4(2):117–124, 1995.

[33] V. Romanov and A. Hasanov. Recovering a potential in damped wave equation from Neumann-to-Dirichlet operator. *Inverse Problems*, 36(115011):30pp, 2020.

[34] J. Singh, P. K. Gupta, and K. N. Rai. Solution of fractional bioheat equations by finite difference method and HPM. *Mathematical and Computer Modelling*, 54(9-10): 2316–2325, 2011.

[35] D. Trucu, D. B. Ingham, and D. Lesnic. Inverse time-dependent perfusion coefficient identification. *Journal of Physics: Conference Series: 4th AIP International Conference and the 1st Congress of the IPIA*, 124(012050):(28 pages), 2008.

[36] D. Trucu, D. B. Ingham, and D. Lesnic. An inverse coefficient identification problem for the bio-heat equation. *Inverse Problems in Science and Engineering*, 17(1):65–83, 2009.

[37] D. Trucu, D. B. Ingham, and D. Lesnic. Inverse temperature-dependent perfusion coefficient reconstruction. *International Journal of Non-Linear Mechanics*, 45(5):542–549, 2010.

[38] D. Trucu, D. B. Ingham, and D. Lesnic. Space-dependent perfusion coefficient identification in the transient bio-heat equation. *Journal of Engineering Mathematics*, 67(4): 307–315, 2010.

[39] D. Trucu, D. B. Ingham, and D. Lesnic. Reconstruction of the space- and time-dependent blood perfusion coefficient in bio-heat transfer. *Heat Transfer Engineering*, 32(9):800–810, 2011.

[40] P. Vernotte. Les paradoxes de la theorie continue de l'equation de la chaleur. *Comptes Rendus de L'Académie Des Sciences*, 246:3154–3155, 1958.

[41] P. Wainwright. Thermal effects of radiation from cellular telephones. *Physics in Medicine & Biology*, 45(8):2363, 2000.

[42] M. Yamamoto. Uniqueness and stability in multidimensional hyperbolic inverse problems. *Journal de Mathématiques Pures et Appliquées*, 78(1):65–98, 1999.